Vietnam Journal of Earth Sciences, 46(3), 322-338, https://doi.org/10.15625/2615-9783/20639

Vietnam Journal of Earth Sciences
https://vjs.ac.vn/index.php/jse

Comparison of Synthetic Aperture Radar Sentinel-1 and ALOS-2 observations for lake monitoring

Binh Pham-Duc

REMOSAT, University of Science and Technology of Hanoi, VAST, Hanoi, Vietnam

Received 21 Jannuary 2024; Received in revised form 8 March 2024; Accepted 22 April 2024

ABSTRACT

This work investigates the efficacy of L-band and C-band Synthetic Aperture Radar (SAR) sensors onboard ALOS-2 and Sentinel-1 satellites, as compared to optical sensors onboard Sentinel-2 satellite, for mapping open water of the Tri An reservoir, one of the largest artificial reservoirs in South Vietnam, during the 2016-2023 period. The Google Earth Engine (GEE) was the primary computing platform to pre-process all satellite observations. The Otsu threshold algorithm was employed to generate water/non-water maps derived from the VH- and HH-polarized backscatter coefficient data acquired by Sentinel-1 and ALOS-2 satellites and from the Modified Normalized Difference Water Index (MNDWI) data acquired by Sentinel-2 satellite, respectively. The findings reveal the stability of Tri An reservoir's surface water extent from 2017 to 2022, followed by a significant decline of nearly 70% during the dry season of 2023 to approximately 100 km^2. This substantial decrease can be explained by the impact of a robust El Niño phase occurring in the region simultaneously. Overall, there is a high consistency between results derived from SAR and optical sensors, but the correlation between Sentinel-1 and Sentinel-2 (R = 0.9774) was higher than that between ALOS-2 and Sentinel-2 (R = 0.9145). During the drought period, both C-band and L-band SAR sensors overestimate the reservoir's surface water extent due to the similarity in their backscatter coefficient between water and dry flat soil surfaces. This misclassification is more pronounced in ALOS-2 data than Sentinel-1 data, suggesting that the C-band sensor is more suitable than the L-band sensor for mapping the lake's open water areas.

Keywords: Lake monitoring; ALOS-2; Sentinel-1; Sentinel-2; Tri An reservoir.

1. Introduction

The Earth's surface is estimated to contain more than 117 million lakes and inland water bodies (Verpoorter et al., 2014) that cover approximately 3% of its land surface (J.A. Downing et al., 2006). Despite their limited spatial coverage, these water bodies have a significant influence on global-scale processes through their impacts on many aspects of the biosphere, such as carbon dioxide and methane emissions (Johnson et al., 2022; Williamson et al., 2009; Zhuang et al., 2023), regulating the balance of regional and global water (Ji et al., 2018), as well as Earth's climate (J. Downing, 2010; Raymond et al., 2013; Tranvik et al., 2009). Furthermore, freshwater from these sources is vital in supporting human health and ecosystem services by providing essentials like drinking water, food, and transportation (Palmer et al., 2015). Under the increasing pressures of climate change and human activities, rapid spatial and temporal transformations of inland water bodies can be witnessed globally (Li, Wang et al., 2022; Woolway et al., 2020; Yao et al., 2023; Zan et al., 2022). Given this changing context, accurate, effective, and

*Corresponding author, Email: pham-duc.binh@usth.edu.vn

timely mapping and monitoring of the transformations of regional and global inland water bodies becomes crucial, especially for environmental monitoring and water management in developing countries (Zhang et al., 2016).

While traditional approaches like conducting field surveys and collecting observations using hydrological monitoring stations provide highly accurate results, they are incredibly time-consuming, challenging in remote areas, and less suitable for long-term monitoring (Li, Ma, et al., 2022). To address these challenges, satellite remote sensing techniques have emerged as a powerful and effective tool for capturing the fast variations of regional and global inland water bodies in near-real time. Optical remote sensing utilizing water indices, such as the Normalized Difference Water Index (NDWI) (Gao, 1996; McFeeters, 1996), the Modified NDWI (MNDWI) (Xu, 2006), or the Automated Water Extraction Index (AWEI) (Feyisa et al., 2014), is widely used for this purpose. Observations acquired from Landsat series, MODIS, and Sentinel-2 satellites are among the most popular free-of-charge data (Asfaw et al., 2020). Several global water distribution datasets have been created using data acquired from these satellites, for instance, the Global Land 30-water 2000 & 2010 (Liao et al., 2014), the Global Surface Wate dataset (Pekel et al., 2016), the ASTER Global Water Body dataset (Abrams et al., 2020), or the Global Inland Water Dynamics (Pickens et al., 2020). However, these datasets (at maximum 30 m spatial resolution) are not always suitable for regional monitoring applications, which require high spatial resolution observations to capture small-scale changes in water bodies. In addition, optical remote sensing is limited in some regions, particularly in the tropics, where the cloud cover usually is very high, especially during rainy seasons. In contrast, radar remote sensing offers an effective solution for monitoring inland water bodies in cloudy regions because their Synthetic Aperture Radar (SAR) sensors emit microwave signals that can penetrate clouds and operate day and night in all weather conditions (Pham-Duc, 2023). Observations acquired by the SAR Sentinel-1A satellite (launched in 2014) were the first radar dataset provided freely to end-users. Since then, SAR data has been used intensively for monitoring inland water bodies (Huth et al., 2020).

Traditionally, users must face the heavy task of downloading satellite observations from space agencies' data hubs and then utilizing specialized software, such as ENVI, ArcGIS, or SNAP to process these observations. This process is time-consuming and demanding, requiring a stable internet connection and high-performance computers, resources often lacking in scholars from numerous developing countries. Thanks to recent technological advancements, cloud computing platforms with supercomputing capabilities offer a significantly faster alternative for processing satellite observations (Pham-Duc, Nguyen, et al., 2023). Among various cloud platforms, Google Earth Engine (GEE), established by Google, stands out as the most popular due to its powerful processing capacity and free accessibility (Gorelick et al., 2017). While Sentinel-1 had long been the unique SAR satellite dataset available in GEE, recently, the Japan Aerospace Exploration Agency (JAXA) decided to release freely the ALOS-2 PALSAR-2 ScanSAR Level 2.2 dataset (Small, 2011), at 25 m pixel spacing, to the community through GEE. This marks the first time two distinct SAR datasets are concurrently available in GEE, providing users with a broader range of options for data selection. This study represents one of the first work focusing on comparing the performance of SAR Sentinel-1 and ALOS-2 observations in mapping inland water bodies. Utilizing cloud-free Sentinel-2 and a few commercial PlanetScope observations as the reference datasets, this study selects the Tri An

reservoir, located in South Vietnam as the test side. The author chose the 2016-2023 period for this study because all satellite observations are accessible during this period.

Details of the study area and all satellite datasets are presented in Section 2. Section 3 focuses on the explanation of the methodology. Results and discussions are presented in Section 4 and Section 5, while Section 6 concludes this study.

2. Study Area and Datasets

2.1. Study Area

Tri An Reservoir (Fig. 1) is one of Vietnam's most significant artificial reservoirs, located in Dong Nai province in South Vietnam (11.152°N and 107.135°E). Commencing its construction in 1984 and finishing in 1987, this water reservoir was designed for multiple purposes, such as flood and drought control, provision of drinking and industrial water, support for agriculture and fisheries activities, and supplying water to the Tri An Hydropower Plant (Nguyen et al., 2020). Under normal conditions, the reservoir has an average depth of 8 m, encompassing an average surface water area of approximately 323 km^2, which allows a total volume of around 2.7×10^6 m^3. Situated in the tropical monsoon climate in South Vietnam, the region experiences an annual mean temperature and precipitation of approximately 33°C and 2400 mm, respectively (Hoang-Cong et al., 2022). The region is characterized by two distinct seasons: the dry season, which accounts for 10-15% of the annual rainfall (December to April), and the rainy season, which accounts for 85-90% of the annual rainfall (May to November) (Pham-Duc et al., 2022).

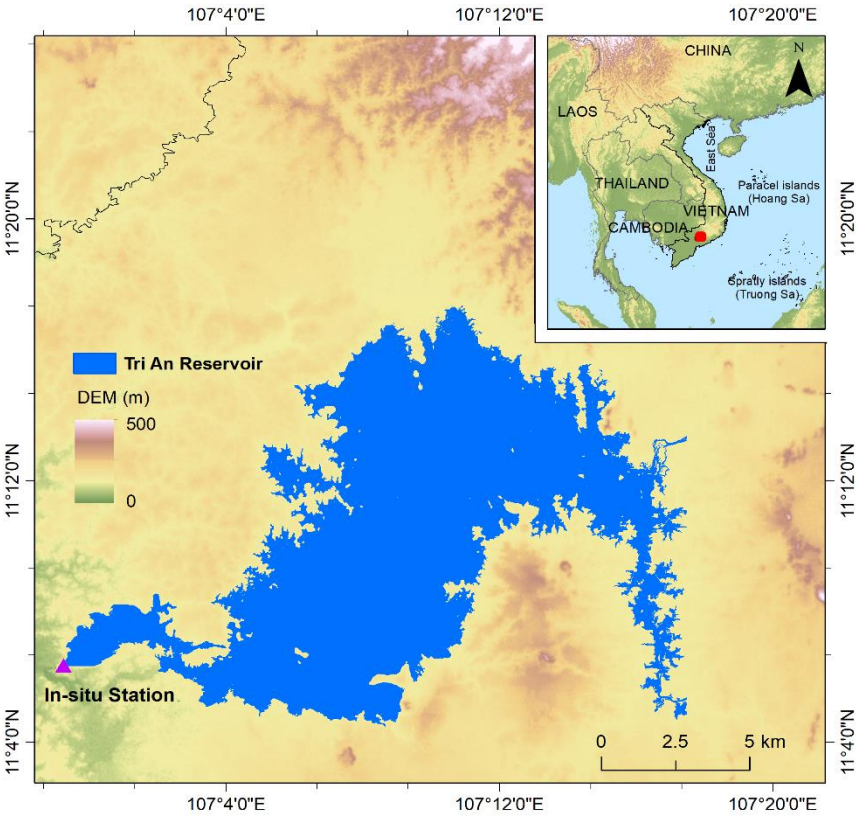

Figure 1. Location of Tri An Reservoir in South Vietnam

2.2. Datasets

The temporal distribution of radar Sentinel-1 and ALOS-2, along with cloud-free Sentinel-2 observations during the 2016-2023 period, which serves as the three satellite datasets for this study, is shown in Fig. 2. The availability of cloud-free observations was limited in 2016, 2017, and 2019; however, in other years, the author could identify between three to six distinct time windows where data from the three satellites were all available. It is worth mentioning that most satellite observations utilized in this study were acquired during the dry season, from December to May, when the prevalence of cloud cover in the region tends to be minimal. In this work, cloud-free Sentinel-2 imagery was utilized as the primary reference dataset to compare the performance and accuracy of radar ALOS-2 and Sentinel-1 imagery for mapping open water areas of lakes.

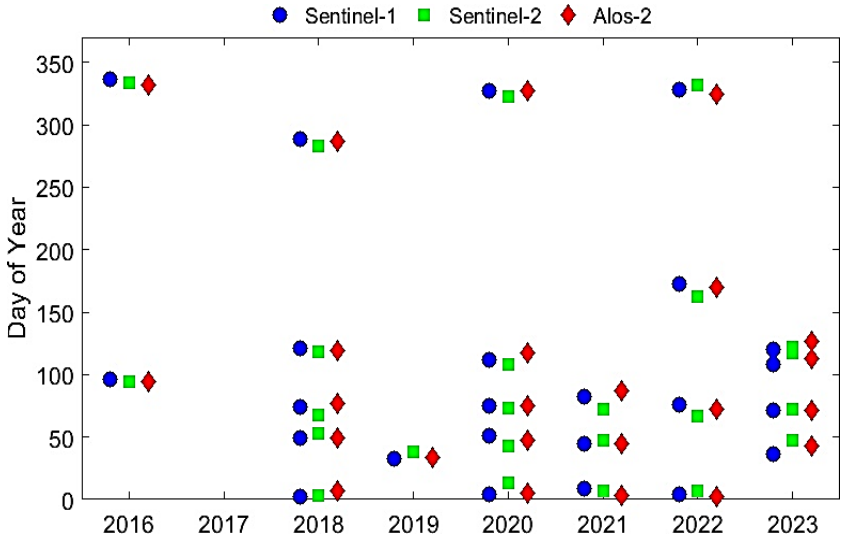

Figure 2. Temporal distribution of all SAR ALOS-2, Sentinel-1, and cloud-free Sentinel-2 satellite observations during 2016-2023, used in this study

2.1.1. SAR Sentinel-1 satellite observations

Sentinel-1 is a radar satellite mission funded by the European Union (EU) and implemented by the European Space Agency (ESA). The mission includes two identical SAR satellites, Sentinel-1A (launched in April 2014) and Sentinel-1-1B (launched in April 2016). Unfortunately, in 2022, ESA had to announce the termination of the Sentinel-1B satellite due to an unexpected anomaly associated with the power supply unit, which is necessary for powering the radar electronics (ESA, 2022). Consequently, only the Sentinel-1A satellite is orbiting the Earth, and efforts are underway to launch the next Sentinel-1C satellite at the earliest opportunity. The two Sentinel-1 satellites orbit in near-polar sun-synchronous orbits at an altitude of 693 km above sea level, with an incidence angle ranging from 29° to 46°. Sentinel-1 sensors operate at C-band (5.405 GHz), providing day-and-night imagery for land and ocean surface applications, with a revisit time of 12 days. This study used 5 m × 20 m spatial resolution VH-polarized Sentinel-1 Ground Range Detected (GRD) L1 imagery acquired in the Interferometric Wide (IW) mode. This satellite product is available on the GEE platform; therefore, all fundamental pre-processing steps of Sentinel-1 data have

already been carried out on the cloud platform. Details of these pre-processing steps, including applying orbit files, thermal noise removal, border noise removal, calibration, and terrain correction, can be found in previous publications (ESA, 2016; Pham Duc & Tong Si, 2021).

2.1.2. Optical Sentinel-2 satellite observations

Sentinel-2 is an optical satellite mission funded by the EU and implemented by the ESA. The mission involves two sun-synchronous satellites orbiting at 786 km above sea level, known as Sentinel-2A (launched in June 2015) and Sentinel-2B (launched in March 2017). The revisit time for each single Sentinel-2 satellite is 10 days, which reduces to 5 days with the combined constellation. The primary instrument of the two satellites is the Multispectral Instrument sensor (MSI), which includes 13 different wavelengths, varying from blue at 500 nm to short wave infrared (SWIR) at 2200 nm. The spatial resolutions provided by Sentinel-2 satellites vary at 10, 20, and 60 m, depending on the wavelengths. Like Sentinel-1, all Sentinel-2 imagery is also accessible in GEE, and all pre-processing steps were conducted in the cloud platform for time-saving. This study utilized Level-2A Bottom-Of-Atmosphere (BOA) reflectance of green and SWIR wavelengths (band 3 and 11, respectively) to calculate the MNDWI. This water index is used later to monitor the variations in the reservoir's water extent.

2.1.3. ALOS-2 satellite observations

The Advanced Land Observing Satellite-2 (ALOS-2), launched in May 2014, is a satellite mission funded by JAXA. ALOS-2 satellite is the follow-on mission of the ALOS satellite (launched in January 2006), with the primary objectives focusing on regional observation, disaster monitoring, land cover classification, and global tropical rainforest monitoring (JAXA, 2023b). ALOS-2 satellite orbits 628 km above the equator in a sun-synchronous sub-recurrent orbit, with an incidence angle of 97.9°. ALOS-2 PALSAR-2 radar sensor operates at L-band (1.2 GHz), with a revisit cycle of 14 days. In this study, HH-polarized PALSAR-2 ScanSAR Level 2.2 product at 25 m pixel spacing, recently added to GEE, was utilized to monitor the reservoir variations. ALOS-2 PALSAR-2 ScanSAR Level 2.2 data was ortho-rectified and radiometrically terrain-corrected before being distributed to GEE; therefore, users only have to conduct a few simple pre-processing steps such as speckle filter and digital-number-to-gamma-naught conversion before moving to the post-processing part (JAXA, 2023a).

2.1.4. In situ data of water level and estimated surface of Tri An Reservoir

Daily in situ measurements of water level and a corresponding table illustrating the relationship between water level and surface water of the reservoir are collected for validation purposes. These datasets are provided by Tri An Hydropower Company (https://trianhpc.vn/). However, it is essential to note that the provided surface water data for Tri An Reservoir was based on statistical estimates dating back to the reservoir's construction and may not perfectly capture the actual dynamics of the reservoir after several decades of deposition within the lake.

3. Methodology

The flowchart of the methodology applied to all radar and optical satellite observations is shown in Fig. 3, which is adapted from previous work (Pham-Duc, 2023; Pham-Duc, Tran Anh, et al., 2023). The VH-polarized Sentinel-1 and HH-polarized ALOS-2 data are selected because these two polarizations are more sensitive than other polarizations in mapping surface water (Gulácsi & Kovács, 2020; Henry et al., 2006). For the Sentinel-1 dataset, each single VH-polarized imagery is spatially subset using a predefined shapefile

(.shp), which fully covers the Tri An Reservoir. Next, the Refined Lee filter is called to reduce speckle noise. The Otsu thresholding algorithm (Otsu, 1979) is applied to the histogram of the processed backscatter coefficient to identify a threshold value to separate each pixel in the Sentinel-1 imagery into non-water (0) or water cluster (1). The binary water/non-water map is then exported to Google Drive and downloaded to a local computer for post-processing. For the ALOS-2 satellite, the pre-processing flowchart is similar to those of Sentinel-1, except that the HH-polarized imagery has been used to generate the binary surface water map of the reservoir. For Sentinel-2 satellite, it is important to remind that only cloud-free observations are used. In the first step, the same predefined shapefile, as for Sentinel-1 and ALOS-2, is utilized to spatially subset the original imagery. Next, the MNDWI map is generated using surface reflectance data of band 3 (green wavelength) and band 11 (SWIR wavelength), then the Otsu method is applied to the MNDWI histogram to classify each pixel into non-water and water clusters. The surface water map is then exported to Google Drive and downloaded to a local computer. For post-processing part, a predefined reservoir's water mask is applied to the resulting binary water/non-water maps, derived from the three satellites during the pre-processing part, to eliminate water bodies not linked to Tri An Reservoir. Finally, the final surface water maps derived from Sentinel-1 (10 m) and ALOS-2 (25 m) satellites are compared to results derived from Sentinel-2 satellites (10 m) to estimate the consistency and accuracy of radar to optical satellite observations in mapping and monitoring Tri An Reservoir's surface water.

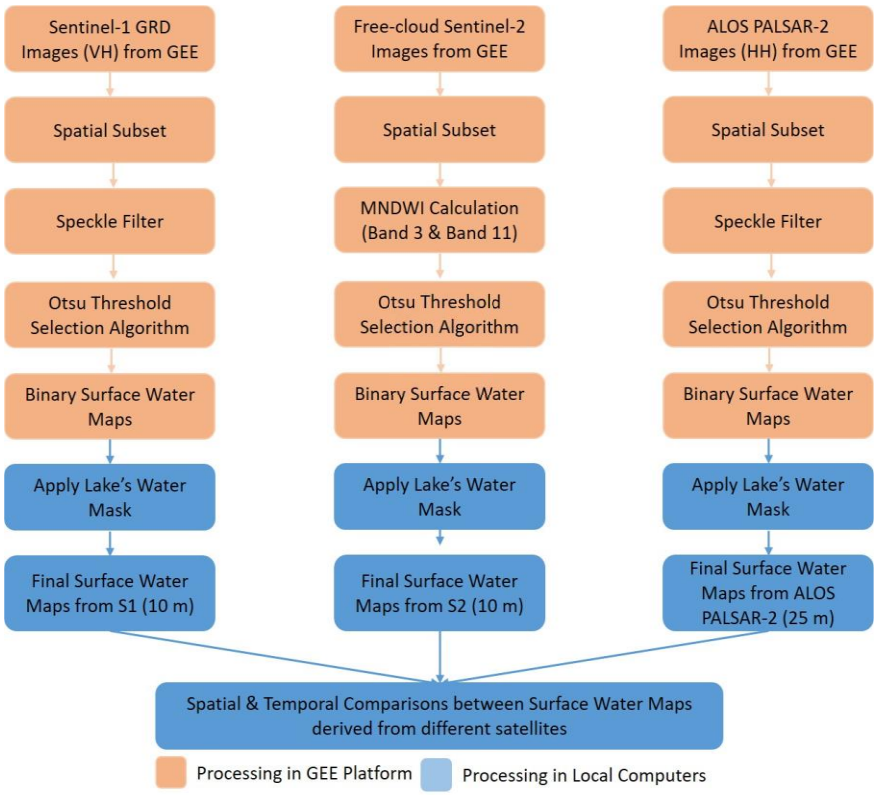

Figure 3. The flowchart utilized in this study is adapted from (Pham-Duc, 2023; Pham-Duc, Tran Anh et al., 2023)

4. Results

4.1. Temporal comparison of surface water maps derived from radar and optical satellites

The temporal dynamics of surface water in Tri An Reservoir during the 2016-2023 period, as derived from the three satellite platforms, along with the estimated surface water areas (derived from in situ water level data), provided by the Tri An Hydropower Company, are shown in Fig. 4. Analysis of results derived from the reference Sentinel-2 data reveals a rapid expansion of the reservoir's water extent, escalating from around 240 km^2 in April 2016 to around 305 km^2 by December 2016. This increase, surpassing 25%, marked the region's termination of the robust 2015/2016 El Niño (Lakshmi et al., 2023). Subsequently, from 2017 to 2022, the reservoir's water exhibited relative stability, oscillating between 280-300 km^2. However, with the onset of another robust El Niño in summer 2023, the reservoir's water extent dropped dramatically by almost 70%, decreasing to approximately 100 km^2 in April/May 2023. This dynamics is validated by comparing its variations with the estimated surface water areas of the reservoir provided by Tri An Hydropower Company (black bars). Although the trend is highly correlated (R = 0.988), the absolute values do not always completely match. As explained above, the reservoir's surface water data was based on statistical estimates dating back to the reservoir's construction nearly four decades ago. By that time, the topography of the reservoir's bottom had changed significantly due to deposition. This explains the difference between results derived from Sentinel-2 observations and values provided by the Tri An Hydropower Company.

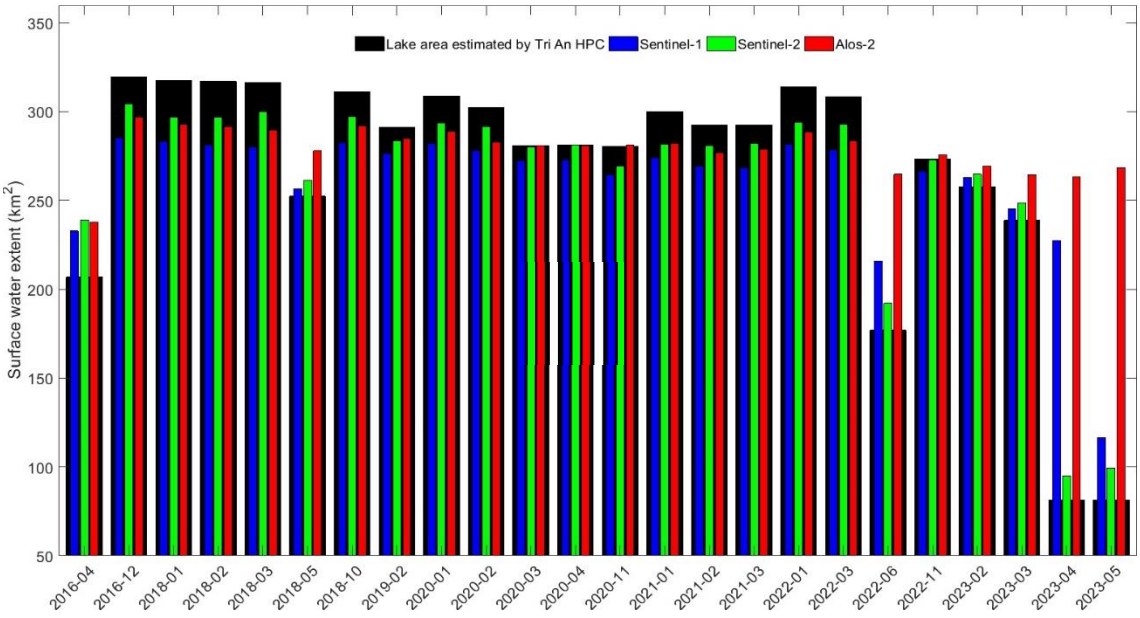

Figure 4. Tri An Reservoir's surface water variations from 2016-2023, derived from the three satellite platforms. Black bars indicate estimated surface water areas derived from in situ water levels provided by Tri An Hydropower Company

Analysis of results derived from radar Sentinel-1 observations shows similar variations of the reservoir dynamics, except in the dry season 2023. During this period, the

Sentinel-1 sensor detected a substantially larger water extent of the reservoir than the reference Sentinel-2 sensor. Conversely, results from the ALOS-2 sensor did not observe a decrease in the reservoir's water extent in summer 2023. This is unexpected as the reservoir's water level in the summer of 2023 hit a 12-year low, as the Tri An Hydropower Company reported. Consequently, the author decided to exclude satellite observations acquired in June 2022, April, and May 2023 from the current analysis due to disparities exceeding 20% of their results. A deeper analysis of satellite observations acquired during these periods is presented in the following subsection to understand why their disparities are abnormal.

The correlations among the remaining 21 pairs of Sentinel-1/Sentinel-2 and ALOS-2/Sentinel-2 are shown in Fig. 5, providing insights into the comparative performance of results derived from these satellite datasets. Notable, the correlation between results derived from Sentinel-1 and the reference Sentinel-2 data (R = 0.9774) is higher than ALOS-2 and Sentinel-2 (R = 0.9145). During this analysis period, the average surface area of the reservoir, as derived from the reference dataset, is around 281.50 km^2, which is 3.83% higher than the number obtained from Sentinel-1 data (270.10 km^2), and only 0.26% higher than that derived from ALOS-2 data (280.80 km^2). It is worth noting that results derived from the Sentinel-1 sensor are consistently lower than results derived from the reference Sentinel-2 sensor. In contrast, results derived from the ALOS-2 sensor fluctuated, being higher in half of the time and lower in the remaining half compared to the reference dataset. This observation suggests that outcomes from the Sentinel-1 sensor exhibit more excellent stability and consistency with the reference Sentinel-2 sensor, emphasizing its reliability in monitoring the dynamics of the reservoir's surface water area compared to the ALOS-2 sensor.

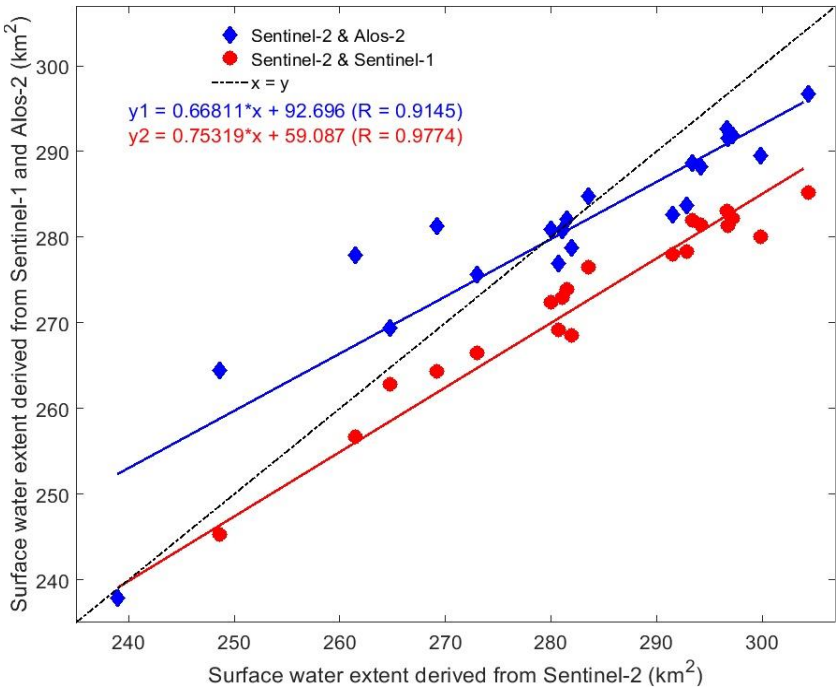

Figure 5. Comparison of Tri An reservoir's surface water, derived from SAR Sentinel-1 and ALOS-2 observations and cloud-free Sentinel-2 observations

4.2. Spatial comparison of surface water maps derived from radar and optical satellites

Figure 6 shows the MNDWI map derived from Sentinel-2, the backscatter coefficient maps derived from Sentinel-1 and ALOS-2 (first column), the resulting surface water extent maps extracted from the three datasets (second column), and the delineation of the reservoir's land/water border derived from the three datasets (third column). All satellite observations were acquired in March 2020 when the disparities between their resulting surface water maps were minimal. Three subfigures in the first column capture the strong contrast between signals reflected from the reservoir and those from the surrounding land. In the MNDWI map, values over water bodies are notably high, typically exceeding 0.6, while values over land surfaces are consistently low, predominantly below -0.5. Examining the backscatter coefficient maps signals over the reservoir range from -28 to 33 dB for Sentinel-1 imagery and -19 to -26 dB for ALOS-2 imagery.

In contrast, signals over land surfaces exhibit considerably higher values, surpassing -18 dB for Sentinel-1 and -16 dB for ALOS-2 imagery, respectively. These distinct lay a favorable foundation for employing the Otsu method in detecting the reservoir's water and land surfaces. The estimated water surface, derived from the reference Sentinel-2 imagery, stands at 279.97 km^2, while estimates from SAR Sentinel-1 and ALOS-2 imagery yield 272.85 and 280.85 km^2, respectively. The differences between results obtained from the reference satellite and the two SAR satellites are only 2.8% and 0.31%, suggesting a remarkable consistency in their results. These discrepancies occur primarily at the east side of the reservoir, where optical Sentinel-2 sensors can detect small branches of the reservoir, but SAR sensors fail to capture them. The land/water border in other reservoir parts is similar to that derived from the three datasets.

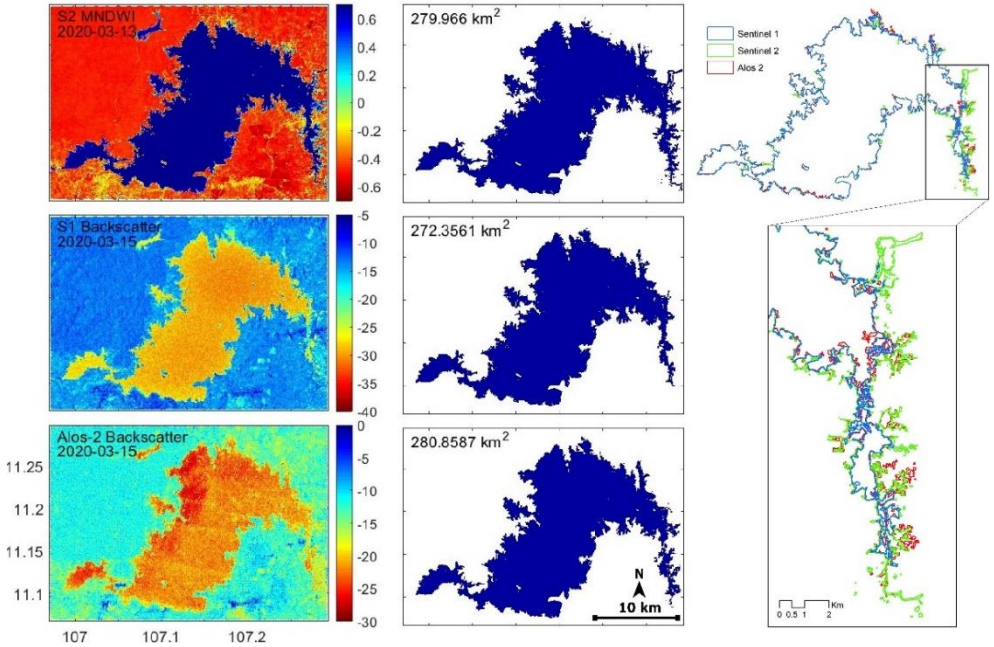

Figure 6. Spatial comparison between surface water maps of Tri An Reservoir, extracted from the three satellite platforms. Sentinel-2 observations were acquired on March 13, 2020, while Sentinel-1 and ALOS-2 observations were acquired on March 15, 2020

5. Discussions on limitations of SAR compared to optical satellite sensors for lake monitoring

The inherent advantages of SAR satellites over optical ones, related to cloud penetration and day-and-night operation, are widely acknowledged in the literature (Xiong et al., 2023). However, this section aims to investigate and discuss a fundamental limitation associated with SAR Sentinel-1 and ALOS-2 satellites compared to optical Sentinel-2 satellites for lake mapping. Specifically, the focus lies on understanding the challenge these SAR sensors face in accurately distinguishing between water surfaces and dry, flat soil surfaces at the bottom of Tri An Reservoir.

The inundation frequency of Tri An Reservoir, derived from all satellite observations acquired from the three platforms during the 2016-2023 period (refer to Fig. 2), is shown in Fig. 7. Results derived from Sentinel-2 observations, considered as the reference dataset, reveal a permanent water area of Tri An Reservoir at approximately 90.45 km^2, accounting for only 32.13% of its mean surface water area. However, results extracted from Sentinel-1 and ALOS-2 observations indicate contrasting figures of 107.90 km^2 and 192.60 km^2, representing a notable 20% and 113% increase compared to the reference dataset. The significant reduction of the permanent surface water of Tri An Reservoir, as observed from Sentinel-2 observations, can be mainly explained by the impact of the robust El Niño occurring in the region during the summer of 2023, which caused a lack of rainfall and a higher temperature (Ngo-Duc, 2023). To validate the accuracy of the reference Sentinel-2 dataset, high-resolution cloud-free observations from commercial PlanetScope SuperDove satellites acquired in April and May 2023 were employed. Figure 8 and Fig. 9 compare the resulting surface water maps of Tri An Reservoir, generated from optical PlanetScope and Sentinel-2, as well as SAR Sentinel-1 and ALOS-2 satellites. In April 2023, due to the effects of drought, the reservoir's surface water was shallow, approximately 93-95 $km^{2,}$ as estimated from optical satellite observations.

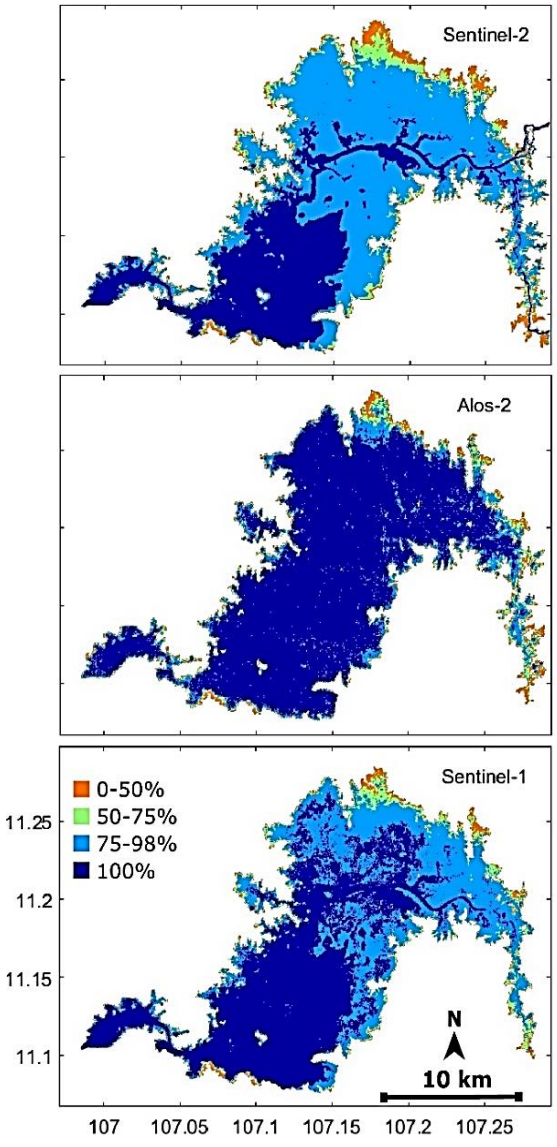

Figure 7. The inundation frequency of the Tri An Reservoir, which was derived from 24 satellite observations acquired from the three platforms during the period 2016-2023

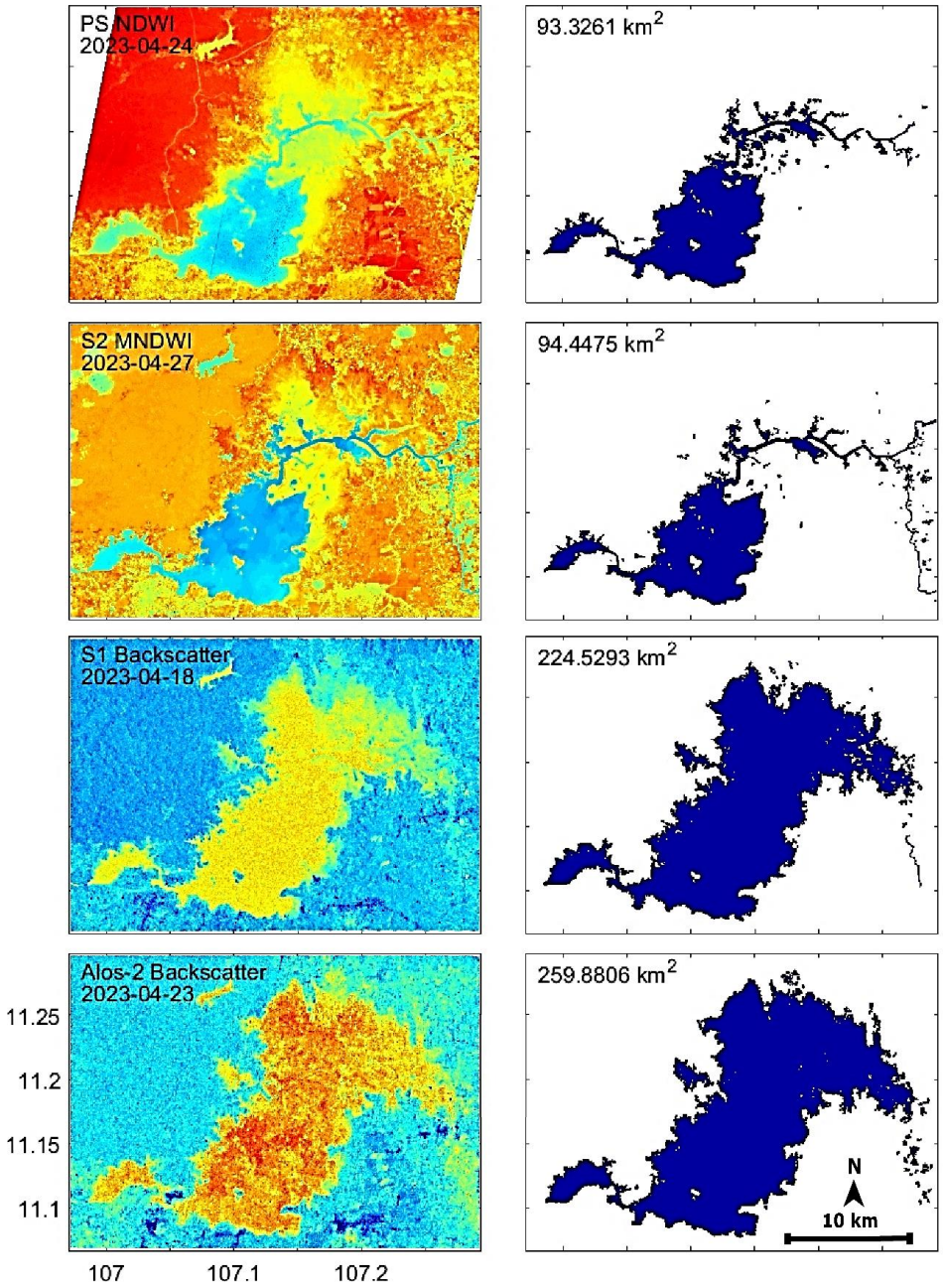

Figure 8. Comparison of surface water extent of Tri An Reservoir, extracted from radar and optical satellite sensors. All satellite observations were acquired in April 2023

In contrast, the Sentinel-1 sensor detected a surface water area of about 224.5 km^2, and ALOS-2 observed nearly 260 km^2. May 2023 continued to show a reduced surface water area as observed from optical satellite imagery (being around 97-99 km^2), while Sentinel-1 and ALOS-2 imagery estimated surface water of approximately 112.60 km^2 and 265.20 km^2, marking a 15% and 170% higher compared to the two reference datasets, respectively. The misclassification in mapping the reservoir's surface water by SAR sensors can be

explained by the similarity in the SAR backscatter coefficient over water and dry, flat soil surface, as discussed in other publications (Pham-Duc, 2023). The elevation of the reservoir and its surroundings is shallow and flat; therefore, during the drought period, when the water recedes, the dry and flat lake bottom mimics water surfaces in reflecting incoming signals from SAR sensors to the specular direction, leading to misclassifications when employing the Otsu method as their backscatter coefficient are highly similar in both VH- and HH-polarized imagery. On the other hand, the clarity of contrast between the reservoir's water surface and its surroundings, as observed in the NDWI and MNDWI maps derived from the reference PlanetScope and Sentinel-2 satellites, enhances the accuracy of their resulting water maps.

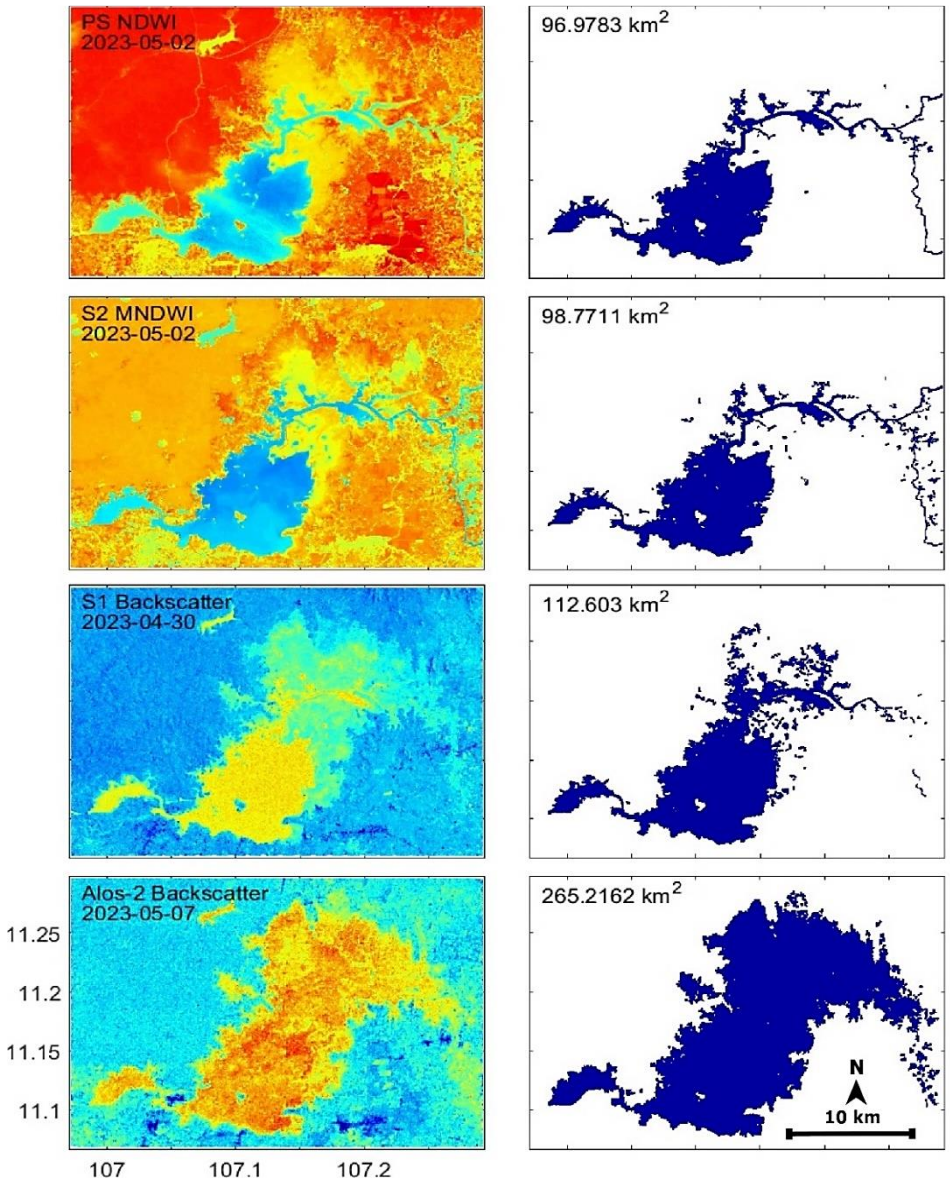

Figure 9. Similar to Fig. 8. All observations were acquired in May 2023

Between April and May 2023, the surface water of Tri An reservoir, estimated using optical satellite observations, slightly changed, but the results estimated using Sentinel-1 observations have reduced by 50%. This problem might be explained by the sensitivity of C-band wavelength with the soil moisture content, which optical remote sensing does not have to face (Shanker Srivastava & Patel, 2022). When water started to withdraw in April due to the drought, the soil was still wet, but it was much drier in May 2023. The difference in soil moisture content affects the interaction of C-band wavelength with the land surfaces, causing significant variations in the retrieved results between the two Sentinel-1 acquisitions.

Another essential point to be discussed is that the overestimation of Tri An reservoir's surface water during the summer of 2023, derived from the ALOS-2 L-band sensor, is much higher than the estimates from the Sentinel-1 C-band sensor. Operating at a wavelength of 23.6 cm, the ALOS-2 sensor exhibits enhanced penetration capabilities, making its observations particularly well-suited for mapping flooded forests. Additionally, the reservoir's bottom is flatter, as observed from the L-band's longer wavelength than the C-band's shorter wavelength, which increases the visual resemblance between the water and flat soil surfaces. This finding aligns with results reported in prior publications, emphasizing the superiority of C-band SAR data over L-band SAR data in the context of lake monitoring (Chen et al., 2020; Ramsey III et al., 2013; Wakabayashi & Nishito, 2015).

6. Conclusions

This study compares the performance of L-band and C-band SAR sensors onboard ALOS-2 and Sentinel-1 satellites to optical sensors onboard Sentinel-2 satellite for mapping open water bodies of Tri An Reservoir, one of the most significant artificial reservoirs in South Vietnam, during the 2016-2023 period. All pre-processing steps of imagery derived from the three satellites were conducted on the GEE cloud computing platform for time-saving. The retrieval water/non-water maps were generated by applying the Otsu threshold algorithm to the VH- and HH-polarized backscatter coefficient maps derived from Sentinel-1 and ALOS-2 data, and MNDWI maps derived from Sentinel-2 data. Findings indicated a consistent surface water of Tri An reservoir from 2017 to 2022, followed by a significant decline of almost 70% of its area, reaching approximately 100 km^2 during the dry season 2023. This decline was partly attributed to a robust El Niño phase occurring concurrently in the region, causing a lack of rainfall and a higher temperature. Overall, a high degree of consistency was observed between SAR and optical data results. However, the correlation between the two Sentinel platforms (R = 0.9774) exceeded that between ALOS-2 and Sentinen-2 (R = 0.9145). During the drought period, both C-band and L-band SAR sensors experience an overestimation of the reservoir's surface water extent due to the resemblances in backscatter coefficients of the water surface, and dry and flat soil surface. More importantly, ALOS-2 data displayed a greater tendency for misclassification than Sentinel-1 data, underscoring the suitability of C-band SAR sensors over L-band SAR sensors for accurately mapping open lake areas, especially during drought periods.

This study is subject to several limitations. First, the lack of a more precise ground truth dataset for comparative analysis against the satellite-derived results poses a challenge. While results extracted from cloud-free Sentinel-2 and PlanetScope observations can serve as the reference datasets, the lack of a more precise ground truth dataset makes it difficult to achieve accurate assessments of

accuracy for each satellite sensor, as in situ data provided by the Tri An Hydropower Company can only validate the temporal dynamics of the reservoir's surface water. Secondly, there is a temporal bias in the acquisition time of satellite imagery. The prevalence of cloud contamination led to over 80% of the satellite observations in this study being acquired during the dry season (between December and April). Consequently, a greater number of imagery acquired during the rainy season is essential to establish a robust conclusion regarding the accuracy and performance of various satellite products. However, accuracy is expected to increase during the rainy season because when the reservoir is fully inundated, it creates a maximal contrast between open water bodies and the surroundings in both SAR and optical satellite observations. Third, Planet Labs granted the author a free account, limiting downloads to less than 5000 km^2 per month. This limitation does not allow the author to use PlanetScope observations as the primary reference dataset in this study.

Acknowledgments

This research was funded by the Vietnam Academy of Science and Technology (VAST), grant number THTEXS.03/22-24 to Binh Pham-Duc. The author expresses gratitude to ESA for providing Sentinel-1 and Sentinel-2 data, JAXA for providing ALOS-2 data, and Planet Labs for providing PlanetScope data, respectively. Special thanks are extended to Do Viet Bach for his invaluable efforts in gathering in situ data from Tri An Hydropower Company. The author thanks the editor and two anonymous reviewers for their valuable comments and suggestions, which significantly improved the quality of the manuscript.

References

Abrams M., Crippen R., Fujisada H., 2020. ASTER Global Digital Elevation Model (GDEM) and ASTER Global Water Body Dataset (ASTWBD). In Remote Sensing, 12, 7. https://doi.org/10.3390/rs12071156.

Asfaw W., Haile A.T., Rientjes T., 2020. Combining multisource satellite data to estimate storage variation of a lake in the Rift Valley Basin, Ethiopia. International Journal of Applied Earth Observation and Geoinformation, 89, 102095. https://doi.org/10.1016/j.jag.2020.102095.

Chen Z., Banks S., Behnamian A., White L., Montpetit B., Pasher J., Duffe J., 2020. Characterizing the Great Lakes Coastal Wetlands with InSAR Observations from X-, C-, and L-Band Sensors. Canadian Journal of Remote Sensing, 46(6), 765–783. https://doi.org/10.1080/07038992.2020.1867974.

Downing J., 2010. Emerging global role of small lakes and ponds: Little things mean a lot. Limnetica, 29, 9–24. https://doi.org/10.23818/limn.29.02.

Downing J.A., Prairie Y.T., Cole J.J., Duarte C.M., Tranvik L.J., Striegl R.G., McDowell W.H., Kortelainen P., Caraco N.F., Melack J.M., Middelburg J.J., 2006. The global abundance and size distribution of lakes, ponds, and impoundments. Limnology and Oceanography, 51(5), 2388–2397. https://doi.org/10.4319/lo.2006.51.5.2388.

ESA, 2016. SAR Basics with the Sentinel-1 Toolbox in SNAP Tutorial. https://step.esa.int/main/doc/tutorials/sentinel-1-toolbox-tutorials/.

ESA, 2022. Mission ends for Copernicus Sentinel-1B satellite. https://www.esa.int/Applications/Observing_the_Earth/Copernicus/Sentinel-1/Mission_ends_for_Copernicus_Sentinel-1B_satellite.

Feyisa G.L., Meilby H., Fensholt R., Proud S.R., 2014. Automated Water Extraction Index: A new technique for surface water mapping using Landsat imagery. Remote Sensing of Environment, 140, 23–35. https://doi.org/10.1016/j.rse.2013.08.029.

Gao B., 1996. NDWI-A normalized difference water index for remote sensing of vegetation liquid water from space. Remote Sensing of Environment, 58(3), 257–266. https://doi.org/10.1016/S0034-4257(96)00067-3.

Gorelick N., Hancher M., Dixon M., Ilyushchenko S., Thau D., Moore R., 2017. Google Earth Engine: Planetary-scale geospatial analysis for everyone. Remote Sensing of Environment, 202, 18–27. https://doi.org/10.1016/j.rse.2017.06.031.

Gulácsi A., Kovács F., 2020. Sentinel-1-Imagery-Based High-Resolution Water Cover Detection on Wetlands, Aided by Google Earth Engine. Remote Sensing, 12(10). https://doi.org/10.3390/rs12101614.

Henry J.-B., Chastanet P., Fellah K., Desnos Y.-L., 2006. Envisat multi-polarized {ASAR} data for flood mapping. International Journal of Remote Sensing, 27(10), 1921–1929. https://doi.org/10.1080/01431160500486724.

Hoang-Cong H., Ngo-Duc T., Nguyen-Thi T., Trinh-Tuan L., Jing Xiang C., Tangang F., Jerasorn S., Phan-Van T., 2022. A high-resolution climate experiment over part of Vietnam and the Lower Mekong Basin: performance evaluation and projection for rainfall. Vietnam J. Earth Sci., 44(1), 92–108. https://doi.org/10.15625/2615-9783/16942.

Huth J., Gessner U., Klein I., Yesou H., Lai X., Oppelt N., Kuenzer C., 2020. Analyzing Water Dynamics Based on Sentinel-1 Time Series a Study for Dongting Lake Wetlands in China. In Remote Sensing, 12, 11. https://doi.org/10.3390/rs12111761.

JAXA, 2023a. ALOS-2 PALSAR-2 ScanSAR Products. https://www.eorc.jaxa.jp/ALOS/en/dataset/palsar2_122_e.htm.

JAXA, 2023b. ALOS-2 Project / ALOS-2 Overview. https://www.eorc.jaxa.jp/ALOS-2/en/about/overview.htm

Ji X., Li Y., Luo X., He D., 2018. Changes in the Lake Area of Tonle Sap: Possible Linkage to Runoff Alterations in the Lancang River? Remote Sensing, 10(6). https://doi.org/10.3390/rs10060866.

Johnson M.S., Matthews E., Du J., Genovese V., Bastviken D., 2022. Methane Emission From Global Lakes: New Spatiotemporal Data and Observation-Driven Modeling of Methane Dynamics Indicates Lower Emissions. Journal of Geophysical Research: Biogeosciences, 127(7), e2022JG006793.

Lakshmi V., Le M.-H., Goffin B.D., Besnier J., Pham H.T., Do H.-X., Fang B., Mohammed I., Bolten J.D., 2023. Regional analysis of the 2015–16 Lower Mekong River basin drought using NASA satellite observations. Journal of Hydrology: Regional Studies, 46, 101362. https://doi.org/10.1016/j.ejrh.2023.101362.

Li J., Ma R., Cao Z., Xue K., Xiong J., Hu M., Feng X., 2022. Satellite Detection of Surface Water Extent: A Review of Methodology. In Water, 14, 7. https://doi.org/10.3390/w14071148.

Li J., Wang J., Yang L., Ye H., 2022. Spatiotemporal change analysis of long time series inland water in Sri Lanka based on remote sensing cloud computing. Scientific Reports, 12(1), 766. https://doi.org/10.1038/s41598-021-04754-y.

Liao A., Chen L., Chen J., He C., Cao X., Chen J., Peng S., Sun F., Gong P., 2014. High-resolution remote sensing mapping of global land water. Science China Earth Sciences, 57(10), 2305–2316. https://doi.org/10.1007/s11430-014-4918-0.

McFeeters S.K., 1996. The use of the Normalized Difference Water Index (NDWI) in the delineation of open water features. International Journal of Remote Sensing, 17(7), 1425–1432. https://doi.org/10.1080/01431169608948714.

Ngo-Duc T., 2023. Rainfall extremes in Northern Vietnam: a comprehensive analysis of patterns and trends. Vietnam J. Earth Sci., 45(2), 183–198. https://doi.org/10.15625/2615-9783/18284.

Nguyen H.-Q., Ha N.-T., Pham T.-L., 2020. Inland harmful cyanobacterial bloom prediction in the eutrophic Tri An Reservoir using satellite band ratio and machine learning approaches. Environmental Science and Pollution Research, 27(9), 9135–9151. https://doi.org/10.1007/s11356-019-07519-3.

Otsu N., 1979. A Threshold Selection Method from Gray-Level Histograms. IEEE Transactions on Systems, Man, and Cybernetics, 9(1), 62–66. https://doi.org/10.1109/TSMC.1979.4310076.

Palmer S.C.J., Kutser T., Hunter P.D., 2015. Remote sensing of inland waters: Challenges, progress and future directions. Remote Sensing of Environment, 157, 1–8. https://doi.org/10.1016/j.rse.2014.09.021.

Pekel J.-F., Cottam A., Gorelick N., Belward A.S., 2016. High-resolution mapping of global surface water and its long-term changes. Nature, 1–19. https://doi.org/10.1038/nature20584.

Pham-Duc B., 2023. Comparison of multi-source

satellite remote sensing observations for monitoring the variations of small lakes: a case study of Dai Lai Lake (Vietnam). Journal of Water and Climate Change, jwc2023505. https://doi.org/10.2166/wcc.2023.505.

Pham-Duc B., Frappart F., Tran-Anh Q., Si S.T., Phan H., Quoc S.N., Le A.P., Viet B. Do, 2022. Monitoring Lake Volume Variation from Space Using Satellite Observations: A Case Study in Thac Mo Reservoir (Vietnam). Remote Sensing, 14(16). https://doi.org/10.3390/rs14164023.

Pham-Duc B., Nguyen H., Phan H., Tran-Anh Q., 2023. Trends and applications of google earth engine in remote sensing and earth science research: a bibliometric analysis using scopus database. Earth Science Informatics, 16(3), 2355–2371. https://doi.org/10.1007/s12145-023-01035-2.

Pham-Duc B., Tran Anh Q., Tong Si S., 2023. Monitoring monthly variation of Tonle Sap Lake water volume using Sentinel-1 imagery and satellite altimetry data. Vietnam J. Earth Sci., 45(4), 479–496. https://doi.org/10.15625/2615-9783/18897.

Pham Duc B., Tong Si S., 2021. Monitoring spatial-temporal dynamics of small lakes based on SAR Sentinel-1 observations: a case study over Nui Coc Lake (Vietnam). Vietnam J. Earth Sci., 44(1), 1–17. https://doi.org/10.15625/2615-9783/16315.

Pickens A.H., Hansen M.C., Hancher M., Stehman S.V, Tyukavina A., Potapov P., Marroquin B., Sherani Z., 2020. Mapping and sampling to characterize global inland water dynamics from 1999 to 2018 with full Landsat time-series. Remote Sensing of Environment, 243, 111792. https://doi.org/10.1016/j.rse.2020.111792.

Ramsey III E., Rangoonwala A., Bannister T., 2013. Coastal Flood Inundation Monitoring with Satellite C-band and L-band Synthetic Aperture Radar Data. JAWRA Journal of the American Water Resources Association, 49(6), 1239–1260. https://doi.org/10.1111/jawr.12082.

Raymond P.A., Hartmann J., Lauerwald R., Sobek S., McDonald C., Hoover M., Butman D., Striegl R., Mayorga E., Humborg C., Kortelainen P., Dürr H., Meybeck M., Ciais P., Guth P., 2013. Global carbon dioxide emissions from inland waters. Nature, 503(7476), 355–359. https://doi.org/10.1038/nature12760.

Shanker Srivastava H., Patel P., 2022. Chapter 22 - Radar remote sensing of soil moisture: fundamentals, challenges & way-out. In P.K. Srivastava, D.K. Gupta, T. Islam, D. Han, & R.B.T.-R.R.S. Prasad (Eds.), Earth Observation. Elsevier, 405–445. https://doi.org/10.1016/B978-0-12-823457-0.00022-7.

Small D., 2011. Flattening Gamma: Radiometric Terrain Correction for SAR Imagery. IEEE Transactions on Geoscience and Remote Sensing, 49(8), 3081–3093. https://doi.org/10.1109/TGRS.2011.2120616.

Tranvik L.J., Downing J.A., Cotner J.B., Loiselle S.A., Striegl R.G., Ballatore T.J., Dillon P., Finlay K., Fortino K., Knoll L.B., Kortelainen P.L., Kutser T., Larsen S., Laurion I., Leech D.M., McCallister S.L., McKnight D.M., Melack J.M., Overholt E., Weyhenmeyer G.A., 2009. Lakes and reservoirs as regulators of carbon cycling and climate. Limnology and Oceanography, 54(6part2), 2298–2314. https://doi.org/10.4319/lo.2009.54.6_part_2.2298.

Verpoorter C., Kutser T., Seekell D.A., Tranvik L.J., 2014. A global inventory of lakes based on high-resolution satellite imagery. Geophysical Research Letters, 41(18), 6396–6402. https://doi.org/10.1002/2014GL060641.

Wakabayashi H., Nishito Y., 2015. Monitoring of tundra lakes with C-band and L-band SAR data. 2015 IEEE International Geoscience and Remote Sensing Symposium (IGARSS), 2076–2079. https://doi.org/10.1109/IGARSS.2015.7326210.

Williamson C.E., Saros J.E., Vincent W.F., Smol J.P., 2009. Lakes and Reservoirs as Sentinels, Integrators, and Regulators of Climate Change. Limnology and Oceanography, 54(6), 2273–2282. http://www.jstor.org/stable/20622831.

Woolway R.I., Kraemer B.M., Lenters J.D., Merchant C.J., O'Reilly C.M., Sharma S., 2020. Global lake responses to climate change. Nature Reviews Earth & Environment, 1(8), 388–403. https://doi.org/10.1038/s43017-020-0067-5.

Xiong Q., Li G., Yao X., Zhang X., 2023. SAR-to-Optical Image Translation and Cloud Removal Based on Conditional Generative Adversarial Networks: Literature Survey, Taxonomy, Evaluation Indicators, Limits and Future Directions. Remote

Sensing, 15(4). https://doi.org/10.3390/rs15041137.

Xu H., 2006. Modification of normalised difference water index (NDWI) to enhance open water features in remotely sensed imagery. International Journal of Remote Sensing, 27(14), 3025–3033. https://doi.org/10.1080/01431160600589179.

Yao F., Livneh B., Rajagopalan B., Wang J., Crétaux J.-F., Wada Y., Berge-Nguyen M., 2023. Satellites reveal widespread decline in global lake water storage. Science, 380(6646), 743–749. https://doi.org/10.1126/science.abo2812.

Zan C., Liu T., Huang Y., Bao A., Yan Y., Ling Y., Wang Z., Duan Y., 2022. Spatial and temporal variation and driving factors of wetland in the Amu Darya River Delta, Central Asia. Ecological Indicators, 139, 108898. https://doi.org/10.1016/j.ecolind.2022.108898.

Zhang Y., Pan M., Wood E.F., 2016. On Creating Global Gridded Terrestrial Water Budget Estimates from Satellite Remote Sensing. Surveys in Geophysics, 37(2), 249–268. https://doi.org/10.1007/s10712-015-9354-y.

Zhuang Q., Guo M., Melack J.M., Lan X., Tan Z., Oh Y., Leung L.R., 2023. Current and Future Global Lake Methane Emissions: A Process-Based Modeling Analysis. Journal of Geophysical Research: Biogeosciences, 128(3), e2022JG007137.